Synthesis of Pb3O4-SiO2-ZnO-WO3 glasses and their fundamental properties for gamma shielding applications

kh. S. Shaaban (khamies1078@yahoo.com)
Al-Azhar University https://orcid.org/0000-0002-5969-3089
E. A Abdel Wahab
Sultan Alomairy
C. Mutuwong
Mohammed Sultan Al-Buriahi

Research Article

Keywords: Silicate glass, micro-hardness, XRD, Structural properties, Gamma shielding

Posted Date: April 21st, 2021

DOI: https://doi.org/10.21203/rs.3.rs-435157/v1

Synthesis of Pb_3O_4-SiO_2-ZnO-WO_3 glasses and their fundamental properties for gamma shielding applications

Kh. S. Shaaban[1], E. A. Abdel Wahab[2], Sultan Alomairy[3], C. Mutuwong[4], M.S. Al-Buriahi[5]

[1]Chemistry Department, Faculty of Science, Al-Azhar University, P.O. 71524, Assiut, Egypt

[2]Physics Department, Faculty of Science, Assiut University, P.O. 71524, Assiut, Egypt

[3]Department of Physics, College of Science, Taif University, P.O.Box 11099, Taif 21944, Saudi Arab

[4] Department of Physics, Ubon Ratchathani University, Ubon Ratchathani, Thailand

[5] Department of Physics, Sakarya University, Sakarya, Turkey

Abstract

In this research, we prepared zinc lead silicate glass system with the composition $35Pb_3O_4$-$60SiO_2$- (5-x) ZnO-xWO_3 ($0 \leq x \leq 5$ mol %) via the melt-quench method. XRD is explored the nature of the glass system. Ultrasonic velocity, and elastic modulus were experimentally investigated and then the results were confirmed by using the theoretical calculations. It was found that because of molar volume reduction inter-ionic distance R_i, polaron radius r_p, and inter-nuclear distance, r_i of the investigated glasses are reduced with WO_3 content. The basic attenuation factors; mass and linear coefficients denoted by μ/ρ and μ, respectively, were determined employing several simulations for each energy via FLUKA code. As WO_3 content increased from 0 to 5 mol %, the μ increased from 0.728 cm^{-1} to 0.856 cm^{-1} achieving high shielding performance for the sample with x = 5 mol %. At 0.6 MeV with x = 5 mol %, we found that the dose rate of the prepared glass system decreases from 2.35×10^7 R/h at 1 mm to 4.71×10^6 R/h at 4 mm. The values of MFP and HVL are lower than those of the conventional photon shields indicating that our prepared glass samples (especially G5 glass sample) have promising shielding properties to use for x/gamma rays applications.

Keywords: Silicate glass; micro-hardness; XRD; Structural properties; Gamma shielding.

1-Introduction

In the various application of glass materials, silicate glass plays an important role due to their unique features like high solubility, high non-linear optical factors, good mechanical moduli, small thermal expansion, and excellent glass-forming domain [1-8]. Moreover, these glasses can be considered as transition metal ion (TMi) to manufacture super-efficient optical and luminescence components. Furthermore, the presence of (TM) in different valences gives the silicate glasses a broad range of scientific and technological importance to use for many applications in various fields [9-17].

In the field of optoelectronic devices, window reflection, thermal and mechanical sensors, attenuation shielding, etc., glasses based on heavy metal oxides (HMO) such as Pb_3O_4, Bi_2O_3, WO_3 and Y_2O_3 have extensive applications [18-29]. HMO glasses have very dense therefore its excellent gamma-ray shielding characteristics. A good candidate for γ-ray shielding applications has been found to be lead containing silicate glasses. Pb_3O_4 are identified as intermediate oxides, or provisional glass modifiers. So, based on the composition of glass, they can act both as network former and network modifier. When its content exceeds 30 mol %, Pb_3O_4 acts as both network former and network modifier in some silicate glasses. As Pb_3O_4 modifies the network of silicate glasses, the silicate structural units can therefore strongly interact with the lead structural unit (PbO_4). One of the so-called non-classical glasses is tungstate glasses. In its compounds, WO_3, can possess six multiple states: 0, +2, +3, +4, +5 and +6. In glass system W it is founded in W^{+3}, W^{+4}, W^{+5} and W^{+6}. The emergence of WO_3 into the glass network enhanced the mechanical and shielding properties of these glasses [30-32].

However, some (HMi) or (TMi) containing glasses exemplify shielding behavior toward more subsequent gamma rays. Several research on radiation impact on multiple doped glasses with different transition metal ions (TMi) have recently been developed by El Batal et al. [33-34]. Among the disguised objectives of several researchers, the specifications of materials that

can serve a double function over the last century can be considered. As a dual function, transparent glasses may be used in radiation shielding materials. Significant numbers of glass research laboratories are increasing day-by-day to develop mechanically transparent radiation shielding glasses [35]. These glasses are used in modern optical devices and in radiation shielding where radiation protection is required.

The glass under studied has become the best substitute for concrete shielding due to its exceptional characteristics such as hardness, chemical stability, and mechanical strength, as well as these glasses, have transparency and mechanical strength. The purposes of this research are to prepare, identify the attenuation proficiency of zinc lead silicate glasses containing different amount of tungstate and identify it is mechanical properties.

2. Preparation the glass samples

Glass samples in Table 1 were formulated using the melt-quench method in the chemical formula $35Pb_3O_4$-$60SiO_2$- (5-x) ZnO-xWO_3 where x: $(0 \geq x \leq 5)$ mol %. SiO_2, Pb_3O_4, ZnO and WO_3 are the initial materials for obtaining these glasses. All the initial materials that have been acquired from Sigma-Aldrich Company. Through grinding the blend repetitively to obtain a fine powder, the starting materials were blended. First, to eliminate H_2O and other impurities, the base materials were heated to 650 °C for 30 min. The heat was increased for 90 minutes to 1150 °C. To reduce the internal stresses, the samples were annealed at 400 C for 3 h and left to cool slowly to ambient temperature.

3. Theoretical background

The glass samples amorphous state was tested and studied via X-ray diffraction (A Philips X-ray diffractometer PW/1710). By using toluene as the immersion liquid, the density of glass samples was estimated by Archimedes' code $\rho = \rho_0 \left(\frac{M}{M-M_1}\right)$ where M and M_1 are the weightings

of air and fluid samples, the glass density is ρ and the density of toluene is ρ_0 (0.865 g. cm^{-1}) with error ±0.001 g cm^{-1}. The molar volume, V_m can be evaluated as $= \frac{M}{\rho}$ where M the molar weight of the glass.

Using the pulse-echo technique, the ultrasonic velocities, longitudinal (v_L) and shear (v_T), at ambient temperature were evaluated. In this method, x-cut and y-cut transducers were used together with KARL DEUTSCH Echograph model 1085 (a digital ultrasonic flaw detector) functioning at 4 MHz with error ±10 m s^{-1}. Besides the density, the velocities have been used to evaluate elastic moduli. longitudinal waves $L = \rho v_L^2$, transverse waves $G = \rho v_T^2$, Young's modulus $Y = (1 + \sigma)2G$, bulk modulus $K = L - \left(\frac{4}{3}\right) G$ [15 − 32].

The elastic moduli of the samples can be evaluated using the exemplary [36, 37] based on packing density $Vi = \left(\frac{3\pi}{4}\right) N_A \, (m\mathrm{R_A^3} + n\,\mathrm{R_O^3})\, m^3.mol^{-1}$, and dissociation energy $Gi = (\frac{1}{V_m}) \sum_i GiXi$, the metallic and oxygen Pauling ionic radii are R_m and R_O. Longitudinal waves $L = K + \left(\frac{4}{3}\right) G$, transverse waves $G = 30 * (\frac{V_i^2 G_i}{V_i})$ Young's modulus $Y = 8.36 V_i G_i$, bulk modulus $K = 10 V_i^2 G_i$. Poission's ratio σ = $\frac{1}{2}$ - $\left(\frac{1}{7.2^* Vi}\right)$. Acoustic Impedance; $Z = v_L \rho$. Micro Hardness; H = $\frac{(1-2\sigma)\mathrm{Y}}{6(1+\sigma)}$. Debye Temperature: $\theta_D = \frac{h}{k}\left(\frac{9N_A}{4\pi V_m}\right)^{\frac{1}{3}} M_s$, Where h and k are the constants of Planck and Boltzmann and N_A is the number of Avogadro.

Average velocities $M_s = \frac{1}{3}\left(\frac{\frac{2}{v_T^3}}{\frac{1}{v_l^3}}\right)^{\frac{1}{3}}$, Thermal coefficient of expansion $\alpha_{P\,=23.2\,(v_L - 0.57457)}$, oxygen molar volume $V_o = \left(\frac{M}{\rho}\right)\left(\frac{1}{\sum xini}\right)$, packing density $OPD = \left(\frac{1000\,C}{Vm}\right)\left(\frac{Mol}{L}\right)$.

4. Monte Carlo technique

Monte Carlo technique is a simulation method for a full description of any experiment in a software environment. In the present study, several Monte Carlo simulations were applied via FLUKA code which is a powerful platform to handle the propagation of radiation (e.g. photons) for a large energy range reaching several hundred MeV [38]. In fact, the FLUKA code is mainly designed to generate the events (collisions) of hadrons in high energy physics. However, since 15 years FLUKA code is used for electromagnetic interactions with high accuracy for estimating the cross sections for photons and electrons. For the present work, we used FLUKA2005.6 version that have a huge library for the photon interactions including coherent process, pair production, and photoelectric effect. Moreover, it is worth mention that different Monte Carlo platforms such as PHITS, Geant4, and MCNP approved their successes to evaluate the photon shielding parameters for several studies [39-45].

5. Results and Discussions

Fig. 1 shows the photographic of the prepared glasses. As exemplified in Fig. 2, no discrete lines, no sharp peaks, were confirmed by XRD patterns and signify that the samples have a high amorphous state. Tungsten ion concentration was calculated as:

$$\mathrm{W}i = \left(\frac{6.023\times10^{23} x\ mol\ fraction\ of\ cation \times valency\ of\ cation}{Vm}\right) \quad (1)$$

It is increases with tungsten ion increased because of molar volume reduction. Quantified inter-ionic distance;

$$R_i = \left(\frac{1}{\text{Concentration of W}}\right)^{\frac{1}{3}} \quad (2)$$

Radius was determined as polaron r_p and internuclear r_i, was calculated as: $rp = \frac{1}{2}\left(\frac{\pi}{6N}\right)^{\frac{1}{3}}, ri = \left(\frac{1}{N}\right)^{\frac{1}{3}}$. W – W separation ($d_{W\text{-}W}$) computed as: $(dW - W) = \left(\frac{V_m^B}{N}\right)^{\frac{1}{3}}$ and $V_m^B = \frac{Vm}{2(1-2Xn)}$. Because of the reduction in molar volume, these have been observed that these characteristics decrease with tungsten. For BO or NBO connection confirmation, the coordinated average number is a

significant criterion and is characterized as $m = \sum n_{ci}\ X_i$ where cation coordination is n_{ci} . Calculate the number of bonds per unit as $n_b = \frac{N_A}{V_m} \sum n_{ci}\ X_i$. These characteristics have been observed to increase with an increase in tungsten oxide content. This results in an increase in the coherence of the glass network and the structure stiffening. All these characteristics, as shown in Table 2.

The changes in the molar volume and density of the glass system are exemplified in Fig. 3. As the WO_3 content increased, the densities of these glasses increased while the molar volume was reduced. Due to the difference in molecular masses between ZnO and WO_3 [81.389 & 231.838], the density increased. Density and molar volume are basically observed to display an inverse correlation. Thus, with increasing tungsten concentration, decreased molar volume values are reported in the present study. The network is therefore more compact, and the glass matrices have increased connectivity. The variations in the oxygen molar volume V_o and oxygen packing density OPD are demonstrated in Fig. 4. The values of V_o have been observed to decrease while the OPD has been increased. Due to the decrease in molar volume, these observations indicate an increase in the number of oxygen bridges (BO).

The velocity of prepared glasses with varying quantities of tungsten oxide has been exemplified in Fig. 5. As shown in Table 3, both velocities (v_L and v_T) were increased with an increase in WO_3 and (v_L) values higher than (v_T). The increase in the evaluated ultrasonic velocity it is possible to explain by considering variables:

(i) Increasing WO_3 will enhance the amorphous network by increasing average coordination number in structural unit.

(ii) Consequently, there was an increased polymerization of the glass coordination number, cross-link density and connectivity within the glass network.

(iii) Because of the increase in internal energy, the velocities were increased.

Experimentally and theoretically, elastic modules were evaluated for prepared glasses and exemplified in Figs 6 and 7. The elastic moduli act exactly as noticed of velocities as exemplified in Figs. 6 and 7 i.e., it depends on the nature of bonds in the glass and the cross-link density. With the increase of WO_3, the elastic moduli values show an increasing trend. The rise in elastic modules as the number of coordinates raised, and heat of formation of W – O (653.1 $KJmol^{-1}$) is higher than Zn – O (284.1 $KJmol^{-1}$), which promotes the development of tungstate glasses rather than zincate. As the modification role of WO_3 in the glass system, all mechanical parameters as revealed in Table 4 are increased with the increase in WO_3 content.

Fig. 8 illustrates a schematic representation for the well-known experiment setup namely; the narrow beam transmission experiment. The geometry of such experiment is an essential block to study and understand the radiation interaction (especially x/gamma rays) with materials. In the present work, we draw this geometry by using FLUKA code. The basic attenuation factors; mass and linear coefficients denoted by μ/ρ and μ, respectively, give a full understanding of photon propagation through mass/linear thickness of an absorbing target. Both μ/ρ and μ were determined employing several simulations for each energy via FLUKA code. The simulations outcomes of these factors were plotted in Fig. 9. Both μ/ρ and μ have similar variation with photon energy, whereas the μ values are higher than those of μ/ρ values. The important difference between μ/ρ and μ is that the μ factor is very helpful to understand the chemical composition dependence of the photon attenuation for the prepared glass specimens. For example, the curve of μ shows that the highest photon attenuation occurs by using G5 glass sample and the lowest photon attenuation occurs by using G1 glass samples. This indicates that the WO_3 addition plays an important role to attenuate the photons beam and then to improve the x/gamma shielding ability of the prepared glass system. More specifically, the maximum μ occurred at 0.6 MeV with the values of 0.728, 0.747, 0.759, 0.796, and 0.856 cm-1 for the prepared glass samples of G1, G2, G3, G4, and G5, respectively. The reason of such increase is the replacement of light metal

oxide (ZnO) by higher one (WO_3). As WO_3 increased from 0 to 5 mol %, the μ increased from 0.728 cm^{-1} to 0.856 cm^{-1}.

Therefore, it is recommended to increase the WO_3 content for getting more superior photon shielding properties of our designed glasses. Our simulation outcomes were numerically confirmed y using XCOM calculations for μ/ρ values. Table 5 listed all the values of μ/ρ obtained by FLUKA simulations and XCOM calculations for each glass sample over the entire considered energy range. Moreover, we listed the deviation (Dev. %) between the FLUKA & XCOM. The Dev. % values were estimated via the relation below:

$$\text{Dev.}(\%) = \frac{(\text{MAC})_{\text{XCOM}} - (\text{MAC})_{\text{FLUKA}}}{(\text{MAC})_{\text{XCOM}}} \times 100 \quad (3)$$

The highest Dev. % was noted at 1.25, 0.6, 1.5, 1.5, and 0.6 MeV with the values of 0.727, 0.923, 0.742, 0.735, and 0.751 for the glass specimens of G1, G2, G3, G4, and G5, respectively. Therefore, the highest Dev. % between FLUKA and XCOM was observed for G2 glass sample with the value of 0.923. Such agreement confirms the accuracy of our simulation outcomes for all the studied parameters in the present work.

The previous interesting observations of the attenuation factors encouraged us taking more deep step to investigate the photon shielding capability of our present glass system. The transmission factors (MFP and HVL) are very important to choose a specific thickness of a material which uses for shielding applications. Moreover, they are usually used for comparing the photon shielding efficiency of new candidates with the conventional photon shields. Fig. 10 shows a description for the photon shielding ability of our prepared glass system in terms of MFP and HVL as a comparison with several photon shields namely; ordinary, hematite-serpentine, ilmenite-limonite, basalt-magnetite, ilmenite, steel-scrap, and steel-magnetite concretes and commercial RS-253-G18 and RS360 glasses. Clearly, the values of MFP and HVL are lower than those of the conventional photon shields indicating that our prepared glass samples (especially

G5 glass sample) have promising shielding properties to use for x/gamma rays applications. Another important factor in the photon attenuation studies is the effective atomic number (Z_{eff}) that is directly related to the partial interactions occurred at different energy regions. Furthermore, the Z_{eff} factor is a main term to determine the effective electron density (N_{eff}) of an absorbing medium. The calculated Z_{eff} & N_{eff} values were plotted as a function of energy for all of the prepared glass specimens as shown in Fig. 11. Obviously, the maximum of Z_{eff} & N_{eff} ($\times 10^{23}$ electron/gram) occurred at energy of 10 MeV with the values of 44.326 & 4.146, 44.378 & 4.147, 44.455 & 4.148, 44.533 & 4.152, and 44.584 & 4.154 for the glass samples of G1, G2, G3, G4, and G5, respectively.

The final task in the present work is the evaluation of the energy absorption factors for each prepared glass sample. The first factor in this task is called specific gamma constant (SGC or Γ) that describes the radioactive source and its exposure in air. The SGC values of the present prepared glass system were evaluated and drawn as a function of WO_3 content for different photon energies namely; 1, 2, 4, and 8 MeV, as shown in Fig. 12. Clearly, the SGC has no significant change by increasing the concentration of WO_3 content at a given photon energy. However, there is a remarkable increase in the values of SGC as the photon energy. Such that the SGC factor increases from the value of about 61 Rm^2/ Ci h at 4 MeV to the value of about 141 Rm^2/ Ci h at 8 MeV. The second factor in this task is called mass energy absorption coefficient (MEAC) that measures the actual absorbed energy by a material (say glass sample). The MEAC factor is of importance in dose rate calculation that is a basic quantity for radiation applications in medicine. Both SGC and MEAC factors were used to calculate the dose rate for each prepared glass sample over the entire considered energy range. Fig. 13 depicts the variation of dose rate (in unit of R/h) with photon energy at several levels of distance in the range between 1 and 15 mm. It is clear that the values of the dose rate vary

from the highest values at the lowest distance (e.g. 1 mm) to the lowest values at the highest distance (e.g. 15 mm). Moreover, one can notice that the rate of reduction in the dose rate was very large between 1 and 5 mm. At 0.6 MeV in the case of G5 glass (as an example), we found that the dose rate decrease from 2.35×10^7 R/h at 1 mm to 4.71×10^6 R/h at 4 mm.

6. Conclusions

Zinc lead silicate glasses containing different amount of tungstate with the formula $35Pb_3O_4$-$60SiO_2$- (5-x) ZnO-xWO_3 where $x: (0 \geq x \leq 5)$ mol % were manufactured using conventional melt-quenching methods. For these glasses, the physical, mechanical, and photon shielding parameters were investigated. The following items were found in the study results:

1- The higher energy formation of W-O bonds than Zn-O is the main reason behind this conclusion which promotes the development of tungstate glasses rather than zincate.

2- The amorphous nature of glasses was established by XRD measurements.

3- The parameters such as density, molar volume, and velocities (v_L and v_T) were measured and then used to determine the mechanical properties of the prepared glass system.

4- Elastic moduli exhibits an increasing trend as WO_3 increases from 0 to 5 mol % and there is a good agreement between the experimental and theoretical elastic moduli.

5- The maximum of Z_{eff} & N_{eff} ($\times 10^{23}$ electron/gram) occurred at energy of 10 MeV with the values of 44.326 & 4.146, 44.378 & 4.147, 44.455 & 4.148, 44.533 & 4.152, and 44.584 & 4.154 for the glass samples of G1, G2, G3, G4, and G5, respectively.

6- The WO_3 content plays an important role to attenuate the photons beam and then to improve the x/gamma shielding ability of the prepared glass system.

7- The specific gamma constant (SGC) has no significant change by increasing the concentration of WO_3 content, while it swiftly increase from 61 Rm^2/ Ci h to 141 Rm^2/ Ci h as photon energy increases from 4 MeV to 8 MeV.

It can be concluded that we successfully introduced a new glass system containing Pb_3O_4, SiO_2, ZnO, and WO_3 with good mechanical properties and potential use in photon shielding applications.

Acknowledgment

We would like to thank Taif University Research Supporting Project number (TURSP-2020/63), Taif University, Taif, Saudi Arabia.

References

[1] Abdel Wahab, E.A., Shaaban, K.S. & Yousef, E.S. (2020), Enhancement of optical and mechanical properties of sodium silicate glasses using zirconia. Opt Quant Electron 52, 458. https://doi.org/10.1007/s11082-020-02575-3

[2] Shaaban, K., Abdel Wahab, E.A., El-Maaref, A.A. *et al.* (2020). Judd–Ofelt analysis and physical properties of erbium modified cadmium lithium gadolinium silicate glasses. J Mater Sci: Mater Electron **31,** 4986–4996 https://doi.org/10.1007/s10854-020-03065-8

[3] E.A. Abdel Wahab, M.S.I. Koubisy, M.I. Sayyed, K.A. Mahmoud, A.F. Zatsepin, Sayed A. Makhlouf, Shaaban, Kh.S. (2021), Novel borosilicate glass system: $Na_2B_4O_7$-SiO_2-MnO_2 Synthesis, average electronics polarizability, optical basicity, and gamma-ray shielding features, Journal of Non-Crystalline Solids, 553,120509, doi.org/10.1016/j.jnoncrysol.2020.120509

[4] El-Rehim, A.F.A., Zahran, H.Y., Yahia, I.S. *et al.* (2020). Physical, Radiation Shielding and Crystallization Properties of Na_2O-Bi_2O_3- MoO_3-B_2O_3- SiO_2 Fe_2O_3 Glasses. Silicon, doi.org/10.1007/s12633-020-00827-1

[5] El-Maaref A.A., Abdel Wahab E.A., Shaaban Kh.S., El-Agmy R.M. (2021), Enhancement of spectroscopic parameters of Er^{3+}-doped cadmium lithium gadolinium silicate glasses as active medium for lasers and optical amplifiers in the NIR-region, Solid State Sciences, doi.org/10.1016/j.solidstatesciences.2021.106539

[6] Wahab, E. A. A., & Shaaban, K. S. (2018). Effects of SnO_2 on spectroscopic properties of borosilicate glasses before and after plasma treatment and its mechanical properties. Materials Research Express, 5(2), 025207, doi:10.1088/2053-1591/aaaee8

[7] Shaaban, K.S., Yousef, E.S., Abdel Wahab, E.A. *et al.* (2020). Investigation of Crystallization and Mechanical Characteristics of Glass and Glass-Ceramic with the Compositions $x$$Fe_2O_3-35SiO_2-35B_2O_3-10Al_2O_3$-(20−$x$) Na_2O. J. of Materi Eng and Perform. https://doi.org/10.1007/s11665-020-04969-6

[8] Somaily, H.H., Shaaban, K.S., Makhlouf, S.A. *et al.* Comparative Studies on Polarizability, Optical Basicity and Optical Properties of Lead Borosilicate Modified with Titania. J Inorg Organomet Polym (2020). https://doi.org/10.1007/s10904-020-01650-2

[9] Saudi, H.A., Abd-Allah, W.M. & Shaaban, K.S. (2020). Investigation of gamma and neutron shielding parameters for borosilicate glasses doped europium oxide for the immobilization of radioactive waste. J Mater Sci: Mater Electron 31(9), 6963-6976, https://doi.org/10.1007/s10854-020-03261-6

[10] Shaaban, K.S., Wahab, E.A.A., Shaaban, E.R. et al. (2020). Electronic Polarizability, Optical Basicity, Thermal, Mechanical and Optical Investigations of ($65B_2O_3$–$30Li_2O$–$5Al_2O_3$) Glasses Doped with Titanate. Journal of Elec Materi 49, 2040–2049. https://doi.org/10.1007/s11664-019-07889-x

[11] Shaaban, K.S., Abo-Naf, S.M. & Hassouna, M.E.M. (2019). Physical and Structural Properties of Lithium Borate Glasses Containing MoO_3. Silicon **11,** 2421–2428 https://doi.org/10.1007/s12633-016-9519-4

[12] Abdel Wahab, E.A., Shaaban, K.S., Elsaman, R. *et al.* (2019). Radiation shielding, and physical properties of lead borate glass doped ZrO_2 nanoparticles. Appl. Phys. A **125,** 869 https://doi.org/10.1007/s00339-019-3166-8

[13] Abd-Allah, W.M., Saudi, H.A., Shaaban, K.S. *et al.* (2019), Investigation of structural and radiation shielding properties of $40B_2O_3$–30PbO–(30-*x*) BaO-*x* ZnO glass system. Appl. Phys. A **125,** 275 https://doi.org/10.1007/s00339-019-2574-0

[14] Shaaban, K. S., Abo-naf S. M., Abd Elnaeim, A. M., & Hassouna, M. E. M. (2017). Studying effect of MoO_3 on elastic and crystallization behavior of lithium diborate glasses. Appl. Phys. A, 123(6), doi:10.1007/s00339-017-1052-9

[15] Shaaban, K.S., Koubisy, M.S.I., Zahran, H.Y. et al. (2020). Spectroscopic Properties, Electronic Polarizability, and Optical Basicity of Titanium–Cadmium Tellurite Glasses Doped

with Different Amounts of Lanthanum. J Inorg Organomet Polym. https://doi.org/10.1007/s10904-020-01640-4

[16] Shaaban, K.S., Yousef, E.S., Mahmoud, S.A. *et al.* (2020). Mechanical, Structural and Crystallization Properties in Titanate Doped Phosphate Glasses. J Inorg Organomet. Polym https://doi.org/10.1007/s10904-020-01574-x

[17] El-Maaref, A. A., Wahab, E. A. A., Shaaban, K. S., Abdelawwad, M., Koubisy, M. S. I., Börcsök, J., & Yousef, E. S. (2020). Visible and mid-infrared spectral emissions and radiative rates calculations of Tm^{3+} doped BBLC glass. Spectrochimica Acta Part A: Molecular and Biomolecular Spectroscopy, 118774. doi: 10.1016/j.saa.2020.118774

[18] Shaaban, K.S., Zahran, H.Y., Yahia, I.S. et al. (2020), Mechanical and radiation-shielding properties of B_2O_3–P_2O_5–Li_2O–MoO_3 glasses. Appl. Phys. A 126, (10), 804. https://doi.org/10.1007/s00339-020-03982-9

[19] El-Sharkawy, R. M., Shaaban, K. S., Elsaman, R., Allam, E. A., El-Taher, A., & Mahmoud, M. E. (2020). Investigation of mechanical and radiation shielding characteristics of novel glass systems with the composition xNiO-20ZnO-60B_2O_3-(20-x) CdO based on nano metal oxides. Journal of Non-Crystalline Solids, 528,119754 doi: 10.1016/j.jnoncrysol.2019.119754

[20] El-Rehim, A.F.A., Shaaban, K.S., Zahran, H.Y. et al. (2020). Structural and Mechanical Properties of Lithium Bismuth Borate Glasses Containing Molybdenum (LBBM) Together with their Glass–Ceramics. J Inorg Organomet Polym https://doi.org/10.1007/s10904-020-01708-1

[21] Shaaban, K.S., Wahab, E.A.A., Shaaban, E.R. et al. (2020). Electronic polarizability, optical basicity and mechanical properties of aluminum lead phosphate glasses. Opt Quant Electron **52,** 125 https://doi.org/10.1007/s11082-020-2191-3

[22] Shaaban, K. S., El Sayed Yousef. (2020), Optical properties of Bi_2O_3 doped boro tellurite glasses and glass ceramics. Optik - International Journal for Light and Electron Optics 203, 163976. https://doi.org/10.1016/j.ijleo.2019.163976

[23] El-Rehim, A.A., Zahran, H., Yahia, I. *et al.* (2020). Radiation, Crystallization, and Physical Properties of Cadmium Borate Glasses. Silicon https://doi.org/10.1007/s12633-020-00798-3

[24] E.A. Abdel Wahab, A.A. El-Maaref, Kh.S. Shaaban, J. Börcsök, M. Abdelawwad, (2020), Lithium cadmium phosphate glasses doped Sm^{3+} as a host material for near-IR laser applications, Optical Materials,110638, https://doi.org/10.1016/j.optmat.2020.110638.

[25] AlBuriahi, M. S., H. H. Hegazy, Faisal Alresheedi, I. O. Olarinoye, H. Algarni, H. O. Tekin, and H. A. Saudi (2020) Effect of CdO addition on photon, electron, and neutron attenuation properties of boro-tellurite glasses. Ceramics International doi.org/10.1016/j.ceramint.2020.10.168

[26] Abouhaswa, A. S., M. H. A. Mhareb, Amani Alalawi, and M. S. Al-Buriahi. (2020) Physical, structural, optical, and radiation shielding properties of B_2O_3-20Bi_2O_3-20Na_2O_2-Sb_2O_3 glasses: Role of Sb_2O_3. Journal of Non-Crystalline Solids 543: 120130. https://doi.org/10.1016/j.jnoncrysol.2020.120130

[27] Naseer, K. A., K. Marimuthu, M. S. Al-Buriahi, Amani Alalawi, and H. O. Tekin. (2020), Influence of Bi_2O_3 concentration on barium-telluro-borate glasses: physical, structural, and radiation-shielding properties. Ceramics International 47, 1: 329-340. https://doi.org/10.1016/j.ceramint.2020.08.138

[28] Abouhaswa, A.S., Al-Buriahi, M.S., Chalermpon, M. *et al.* (2020), Influence of ZrO_2 on gamma shielding properties of lead borate glasses. *Appl. Phys. A* **126,** 78. https://doi.org/10.1007/s00339-019-3264-7

[29] Gokhan Kilic, F.I.El Agawany, Buse Ozen Ilik, K.A. Mahmoud, Erkan Ilik, Y.S. Rammah, (2021),Ta_2O_5 reinforced Bi_2O_3–TeO_2–ZnO glasses: Fabrication, physical, structural characterization, and radiation shielding efficacy, Optical Materials, 112, 110757, ttps://doi.org/10.1016/j.optmat.2020.110757.

[30] Stalin, Salavadi, D. K. Gaikwad, M. S. Al-Buriahi, Ch Srinivasu, Shaik Amer Ahmed, H. O. Tekin, and Syed Rahman. (2020) Influence of Bi_2O_3/WO_3 substitution on the optical, mechanical, chemical durability and gamma ray shielding properties of lithium-borate glasses. Ceramics International https://doi.org/10.1016/j.ceramint.2020.10.109

[31] ElBatal H.A.; Abdelghany A.M.; F.H. ElBatal, EzzElDin F.M. (2012). Gamma rays interactions with WO_3-doped lead borate glasses. 134(1), 542 548. doi: 10.1016/j.matchemphys.2012.03.032

[32] Kaur, Arshpreet; Khanna, Atul; Sathe, Vasant G.; Gonzalez, Fernando; Ortiz, Belen (2013). Optical, thermal, and structural properties of Nb_2O_5–TeO_2 and WO_3–TeO_2 glasses. Phase Transitions, 86(6), 598–619. doi:10.1080/01411594.2012.727998

[33] ElBatal, F.H., Marzouk, S.Y. (2009). Interactions of gamma rays with tungsten-doped lead phosphate glasses. *J Mater Sci* **44,** 3061–3071 https://doi.org/10.1007/s10853-009-3406-y

[34] Fayad, A.M., Ouis, M.A., ElBatal, F.H. *et al.* (2018). Shielding Behavior of Gamma-Irradiated MoO_3 or WO_3-Doped Lead Phosphate Glasses Assessed by Optical and FT Infrared Absorption Spectral Measurements. Silicon **10,** 1873–1879 https://doi.org/10.1007/s12633-017-9692-0

[35] Kaewjaeng, S., Kothan, S., Chaiphaksa, W., Chanthima, N., Raja Ramakrishna, R., Kim, H. J., & Kaewkhao, J. (2019), High transparency La_2O_3-CaO-B_2O_3-SiO_2 glass for diagnosis x-rays shielding material application, Radiation Physics and Chemistry, 160,41-47, 10.1016/j.radphyschem.2019.03.018

[36] Makishima, A. and J.D. Mackenzie, Direct calculation of Young's modulus of glass. Journal of Non-Crystalline Solids, **12**(1), 35-45. (1973). https://doi.org/10.1016/0022-3093(73)90053-7

[37] Makishima, A. and J.D. Mackenzie, Calculation of bulk modulus, shear modulus, and Poisson's ratio of glass. Journal of Non-crystalline solids, **17**(2) 147-157. (1975). https://doi.org/10.1016/0022-3093(75)90047-2

[38] Battistoni, Giuseppe, F. Cerutti, A. Fasso, A. Ferrari, S. Muraro, J. Ranft, S. Roesler, and P. R. Sala. "The FLUKA code: Description and benchmarking." In *AIP Conference proceedings*, vol. 896, no. 1, pp. 31-49. American Institute of Physics, 2007.

[39] AlBuriahi, M. S., H. H. Hegazy, Faisal Alresheedi, I. O. Olarinoye, H. Algarni, H. O. Tekin, and H. A. Saudi. (2020).Effect of CdO addition on photon, electron, and neutron attenuation properties of boro-tellurite glasses. Ceramics International https://doi.org/10.1016/j.ceramint.2020.10.168

[40] Stalin, Salavadi, D. K. Gaikwad, M. S. Al-Buriahi, Ch Srinivasu, Shaik Amer Ahmed, H. O. Tekin, and Syed Rahman. Influence of Bi_2O_3/WO_3 substitution on the optical, mechanical, chemical durability and gamma ray shielding properties of lithium-borate glasses. Ceramics International (2020). https://doi.org/10.1016/j.ceramint.2020.10.109

[41] Al-Buriahi, M. S., Y. S. M. Alajerami, A. S. Abouhaswa, Amani Alalawi, Tanin Nutaro, and Baris Tonguc. (2020): Effect of chromium oxide on the physical, optical, and radiation shielding properties of lead sodium borate glasses. Journal of Non-Crystalline Solids 544 120171. https://doi.org/10.1016/j.jnoncrysol.2020.120171

[42] Naseer, K. A., K. Marimuthu, M. S. Al-Buriahi, Amani Alalawi, and H. O. Tekin. (2020), Influence of Bi_2O_3 concentration on barium-telluro-borate glasses: physical, structural and radiation-shielding properties. Ceramics International 47, 1: 329-340. https://doi.org/10.1016/j.ceramint.2020.08.138

[43] Boukhris, Imed, Imen Kebaili, M. S. Al-Buriahi, Amani Alalawi, A. S. Abouhaswa, and Barıs Tonguc. (2020): Photon and electron attenuation parameters of phosphate and borate

bioactive glasses by using Geant4 simulations. Ceramics International 46, 15, 24435-24442. https://doi.org/10.1016/j.ceramint.2020.06.226

[44] Al-Buriahi, M. S., Esraa M. Bakhsh, Barıs Tonguc, and Sher Bahadar Khan. Mechanical and radiation shielding properties of tellurite glasses doped with ZnO and NiO. Ceramics International (2020). https://doi.org/10.1016/j.ceramint.2020.04.240

[45] Al-Buriahi, M. S., V. P. Singh, Amani Alalawi, Chahkrit Sriwunkum, and Baris Tamer Tonguc. (2020),Mechanical features and radiation shielding properties of TeO_2–Ag_2O-WO_3 glasses. Ceramics International . https://doi.org/10.1016/j.ceramint.2020.03.091

Figures

Figure 1

Photographic of the prepared glasses.

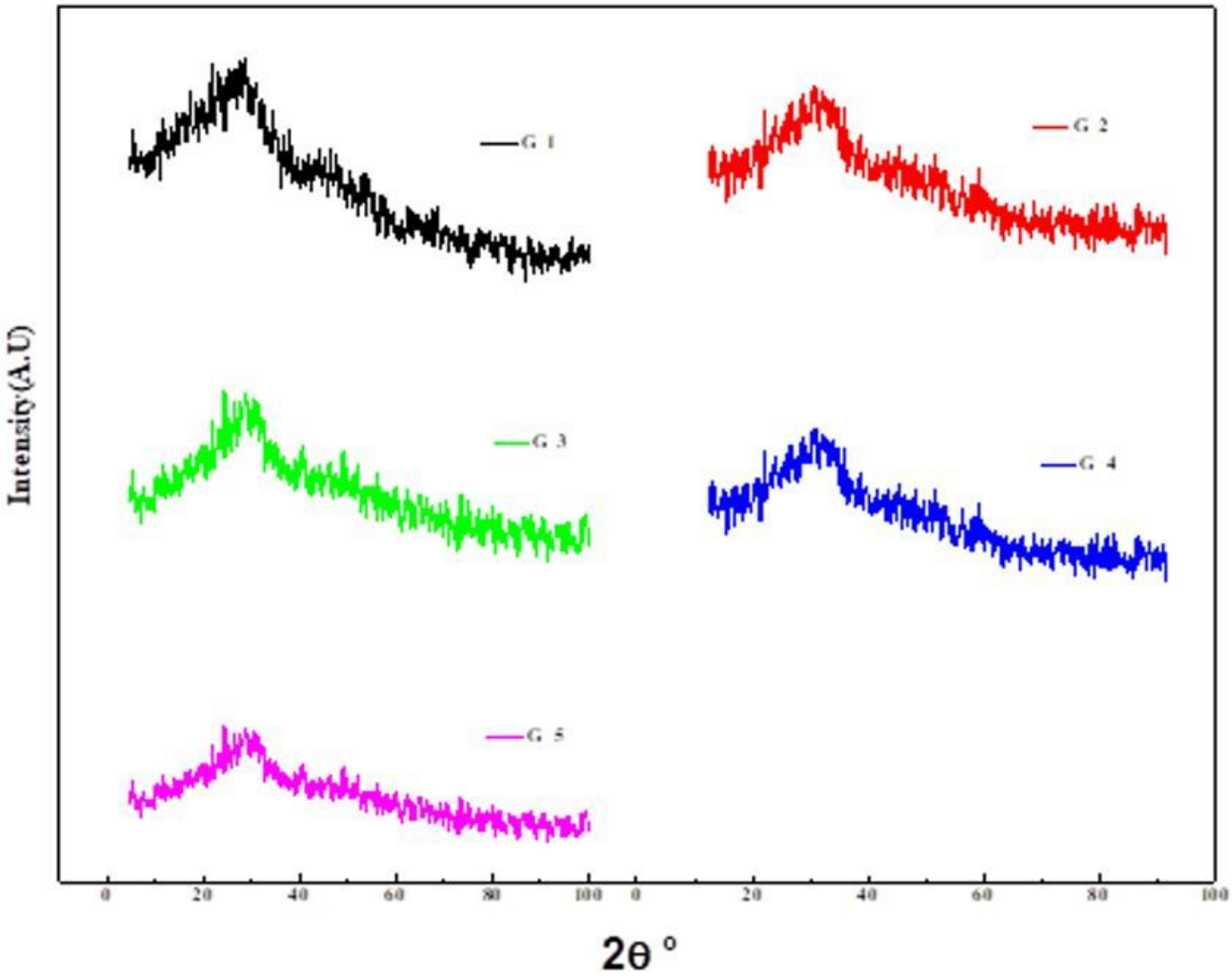

Figure 2

XRD of the prepared glasses.

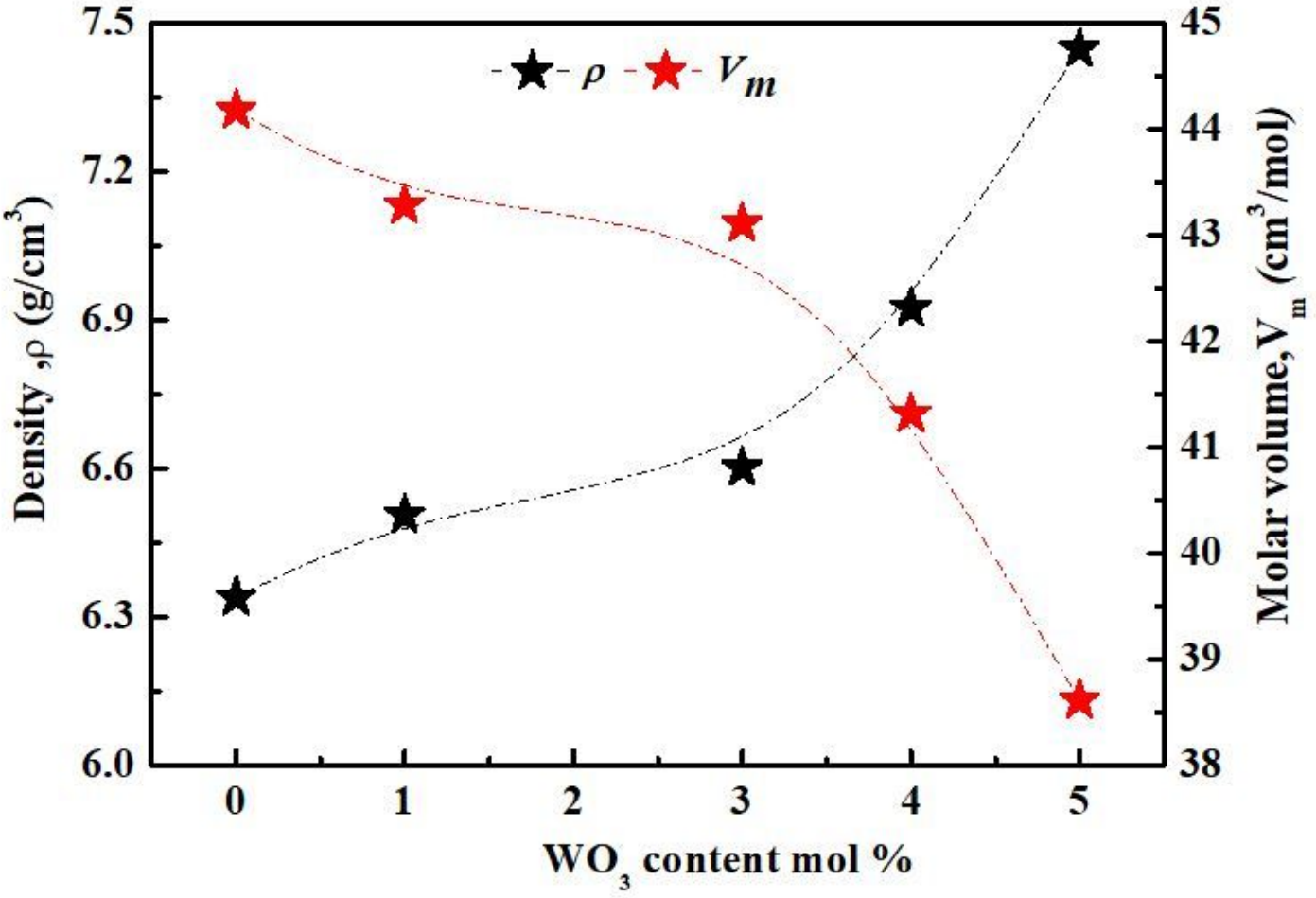

Figure 3

Glass density and molar volume as a function of WO3 content.

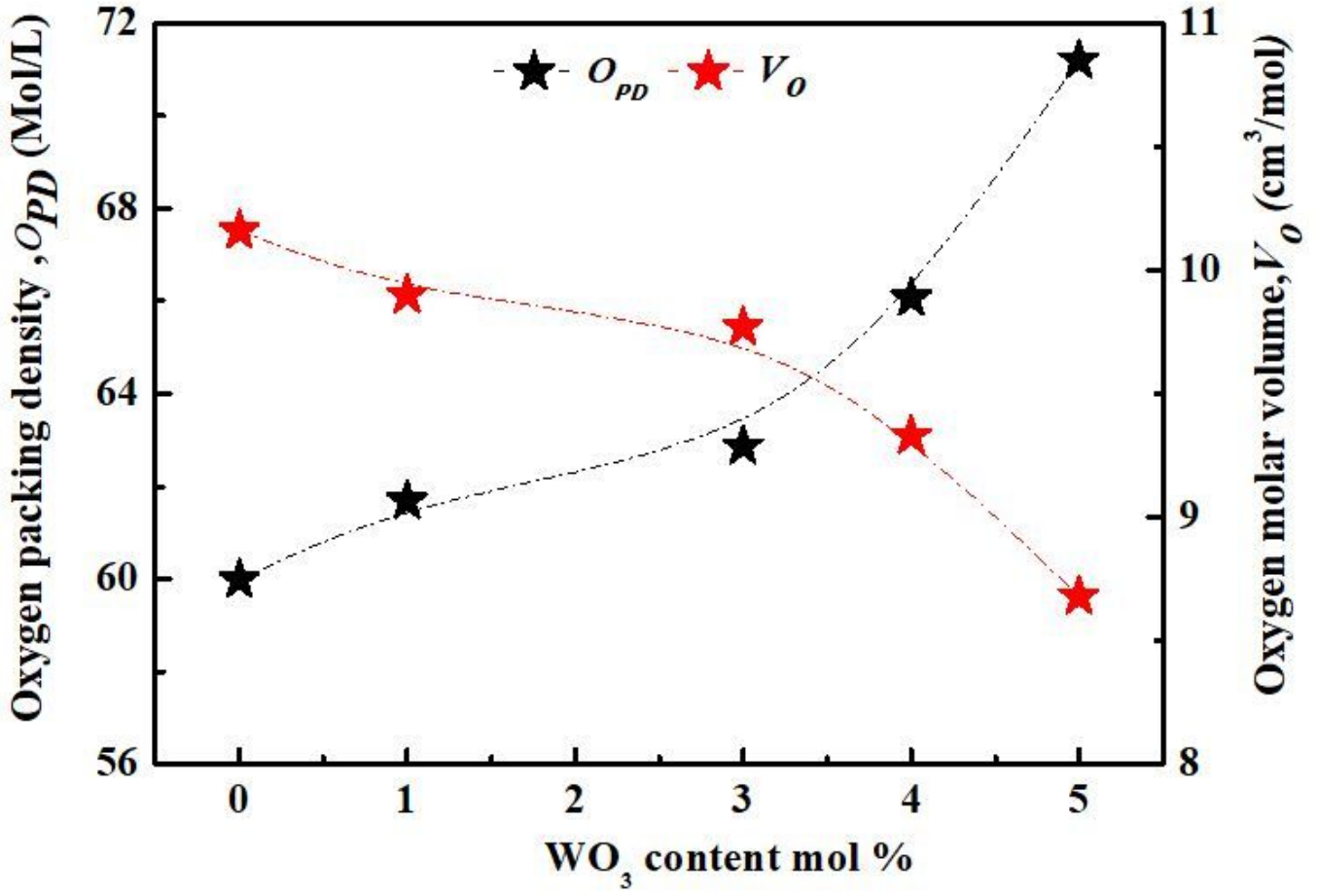

Figure 4

Oxygen packing density and oxygen molar volume as a function of WO3 content.

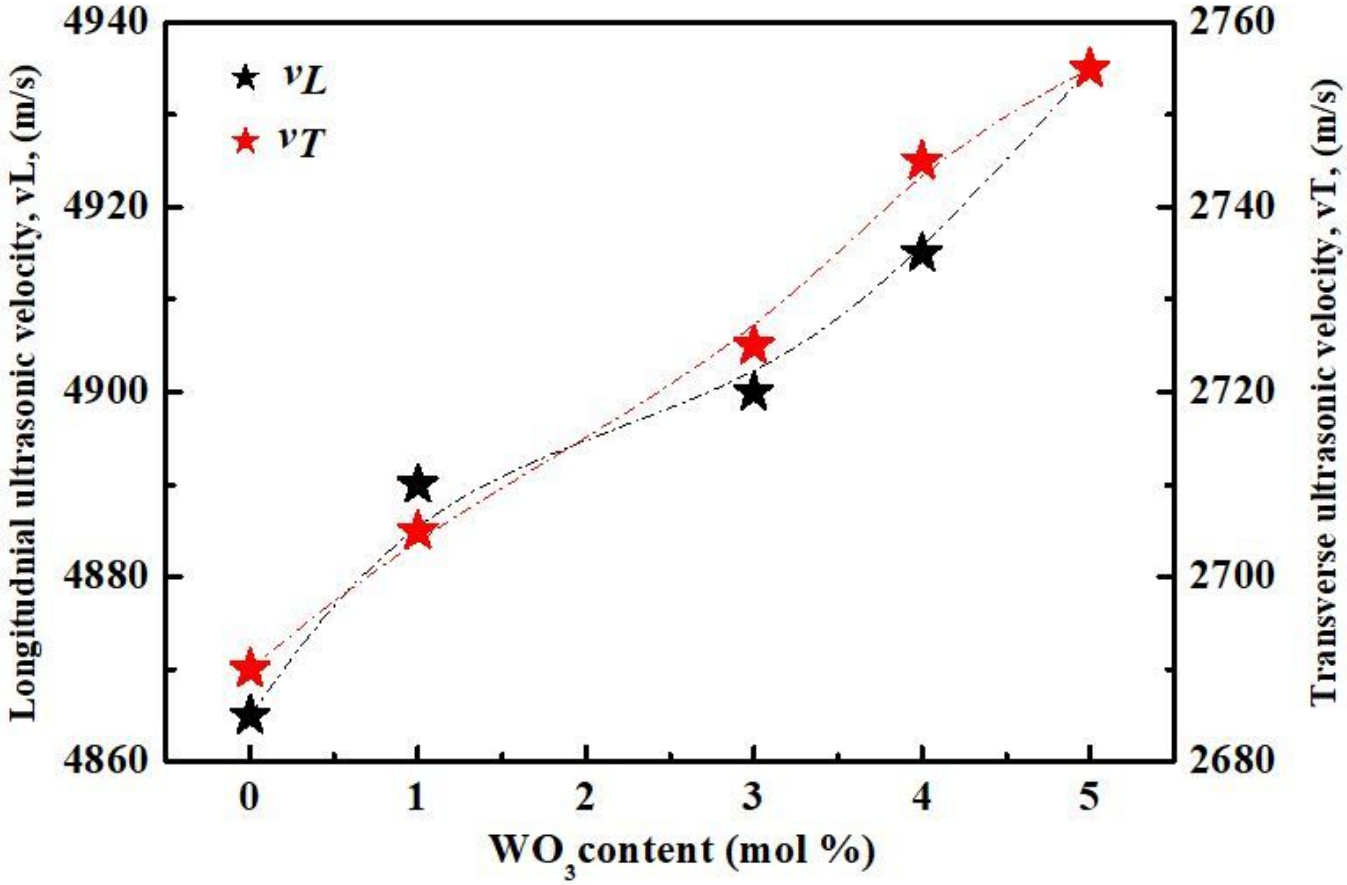

Figure 5

Ultrasonic velocities of prepared glasses with varying quantities of WO3.

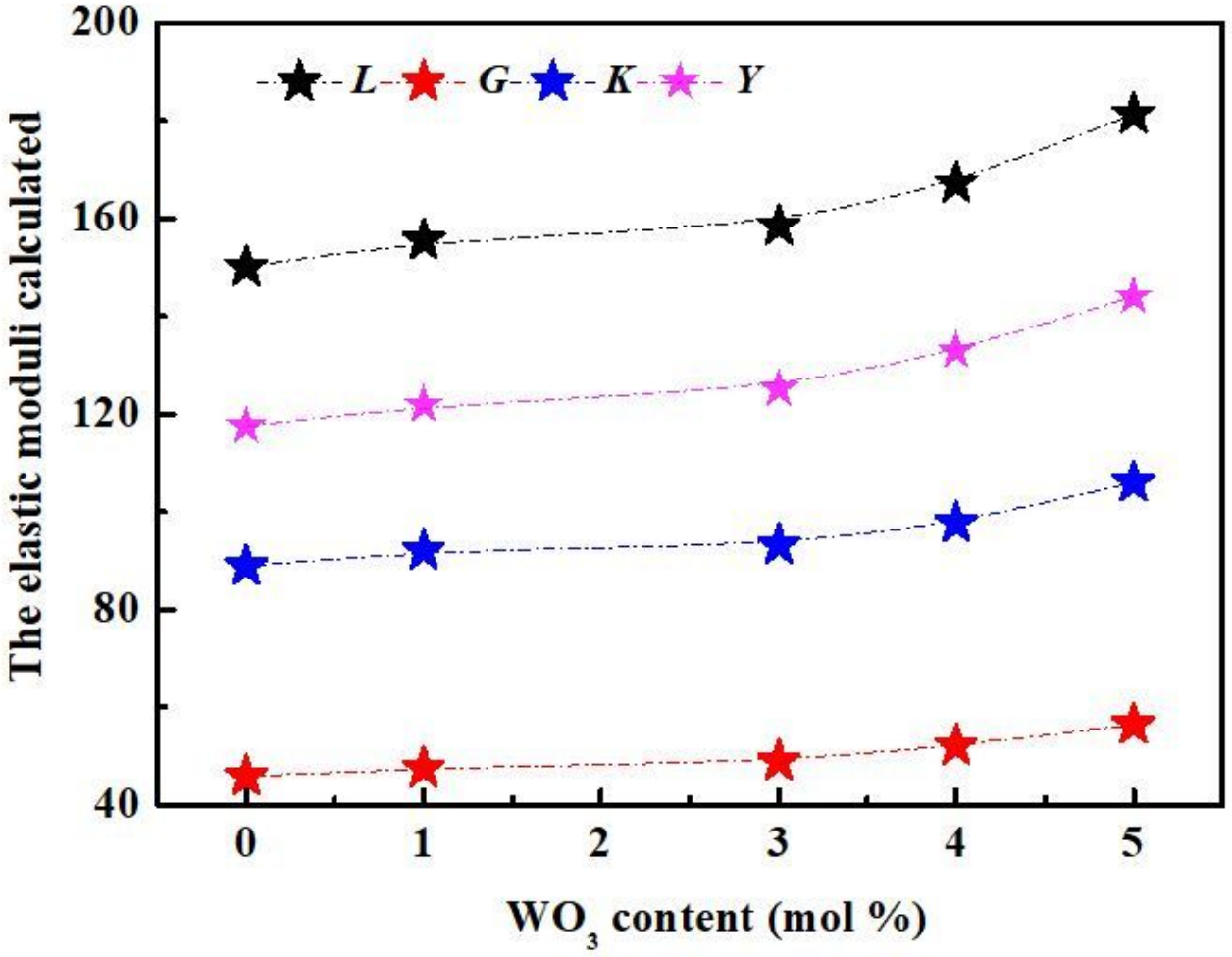

Figure 6

Experimental elastic modules of prepared glasses with varying quantities of WO3.

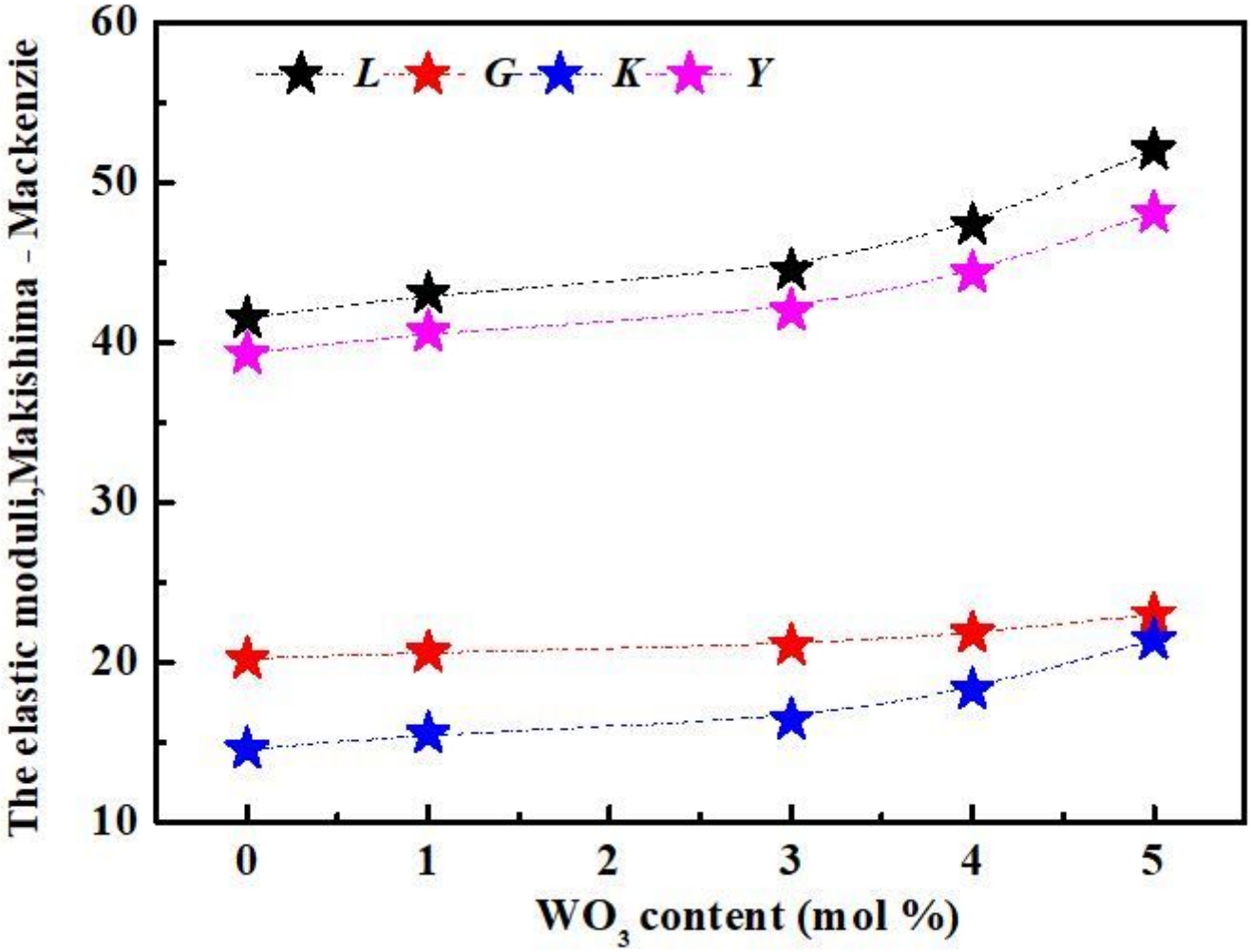

Figure 7

Theoretical elastic modules of prepared glasses with varying quantities of WO3.

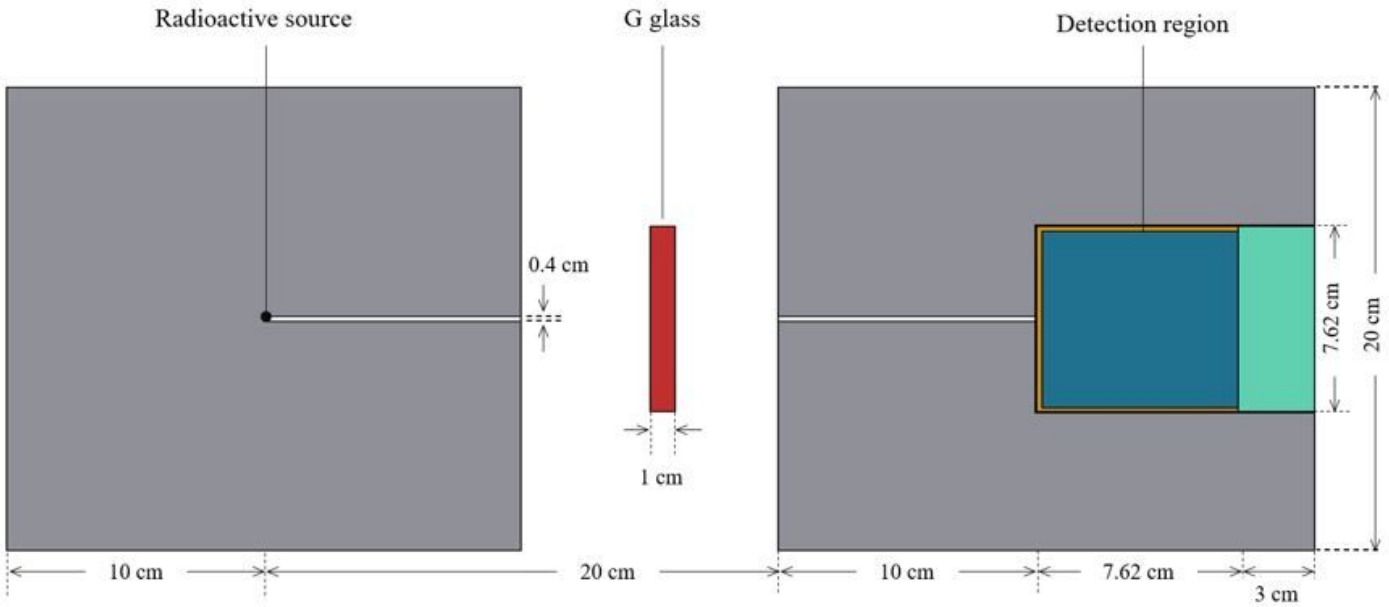

Figure 8

Schematic representation of the narrow beam transmission geometry drawn in the present work using FLUKA code.

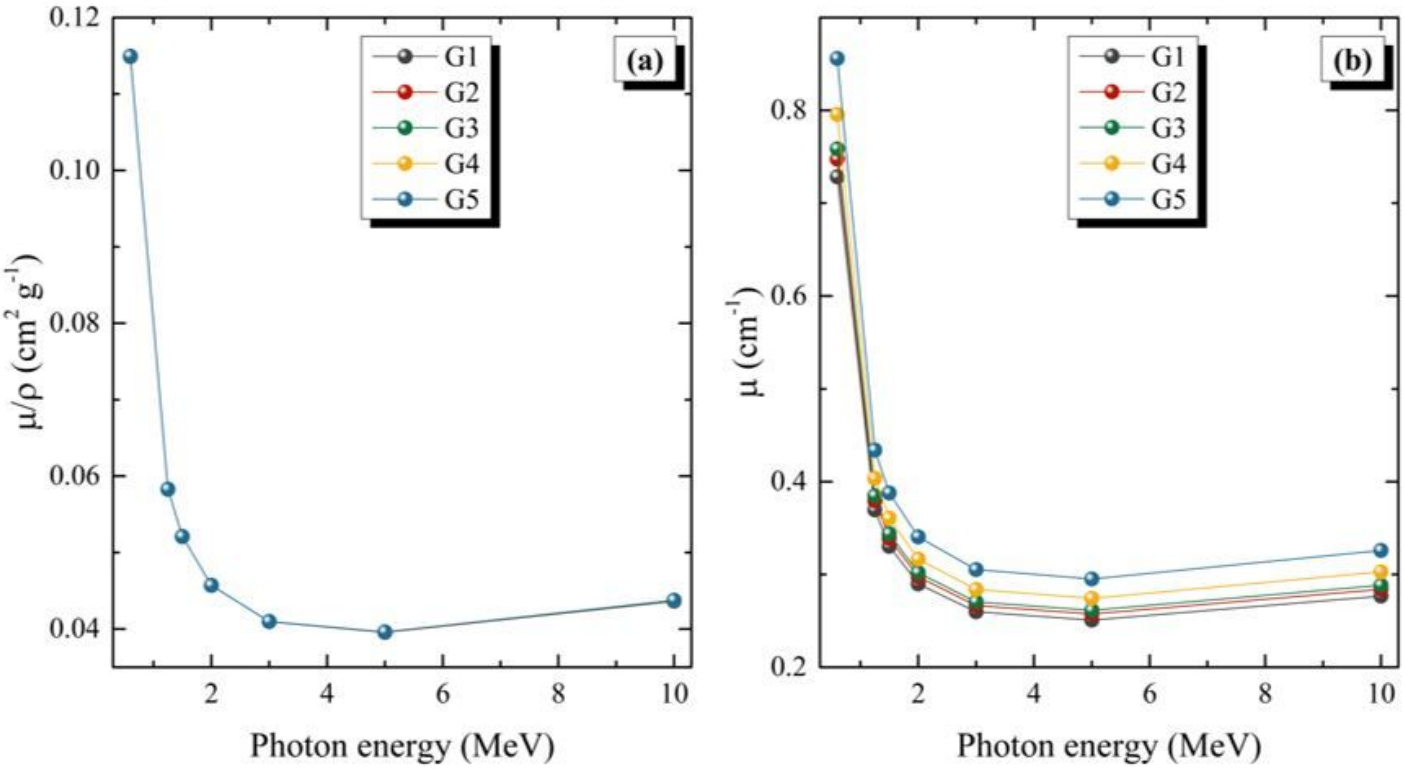

Figure 9

Photon energy dependence of the linear and mass attenuation coefficients for the SiO2–Pb3O4–ZnO–WO3 glasses.

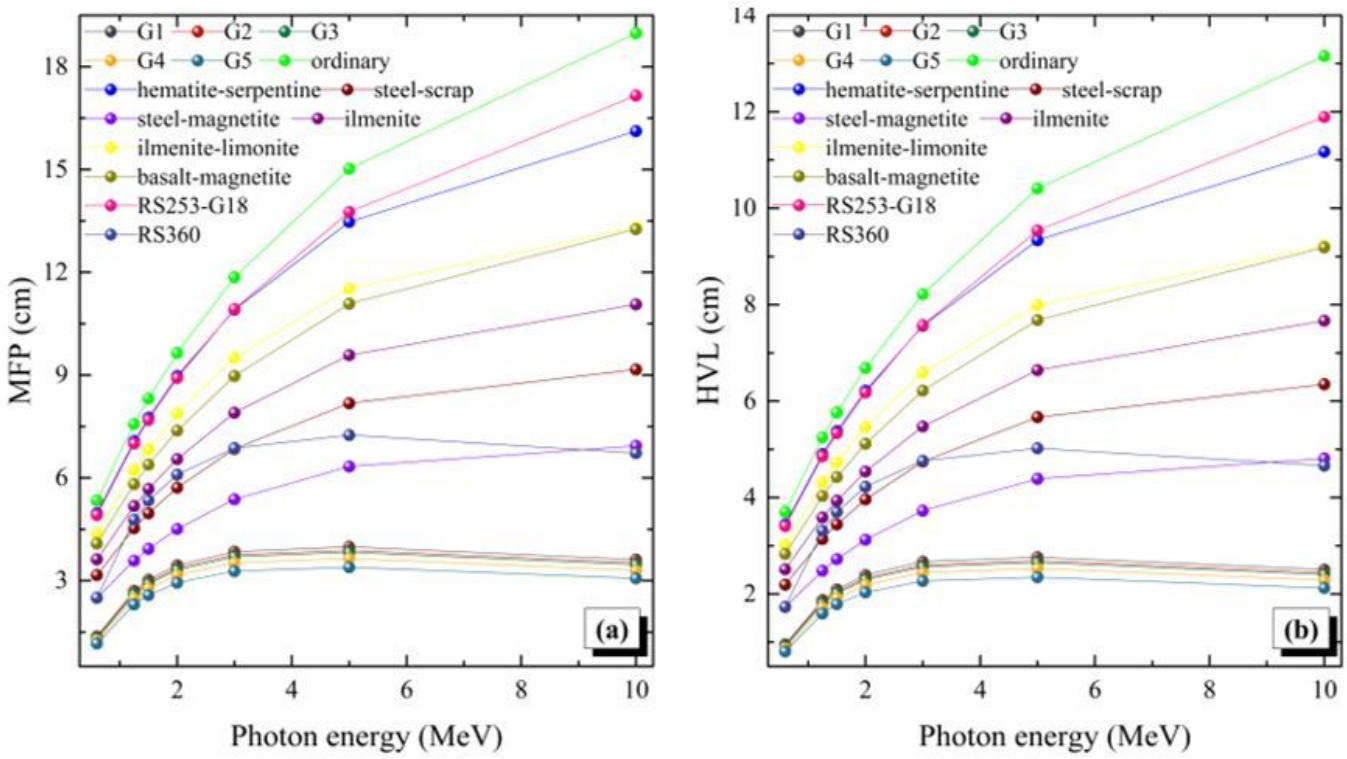

Figure 10

Variations of mean free path and half value layer as a function of photon energy for the SiO2–Pb3O4–ZnO–WO3 glasses in comparison to ordinary, hematite-serpentine, ilmenite-limonite, basalt-magnetite, ilmenite, steel-scrap, and steel-magnetite concretes and commercial RS-253-G18 and RS360 glasses.

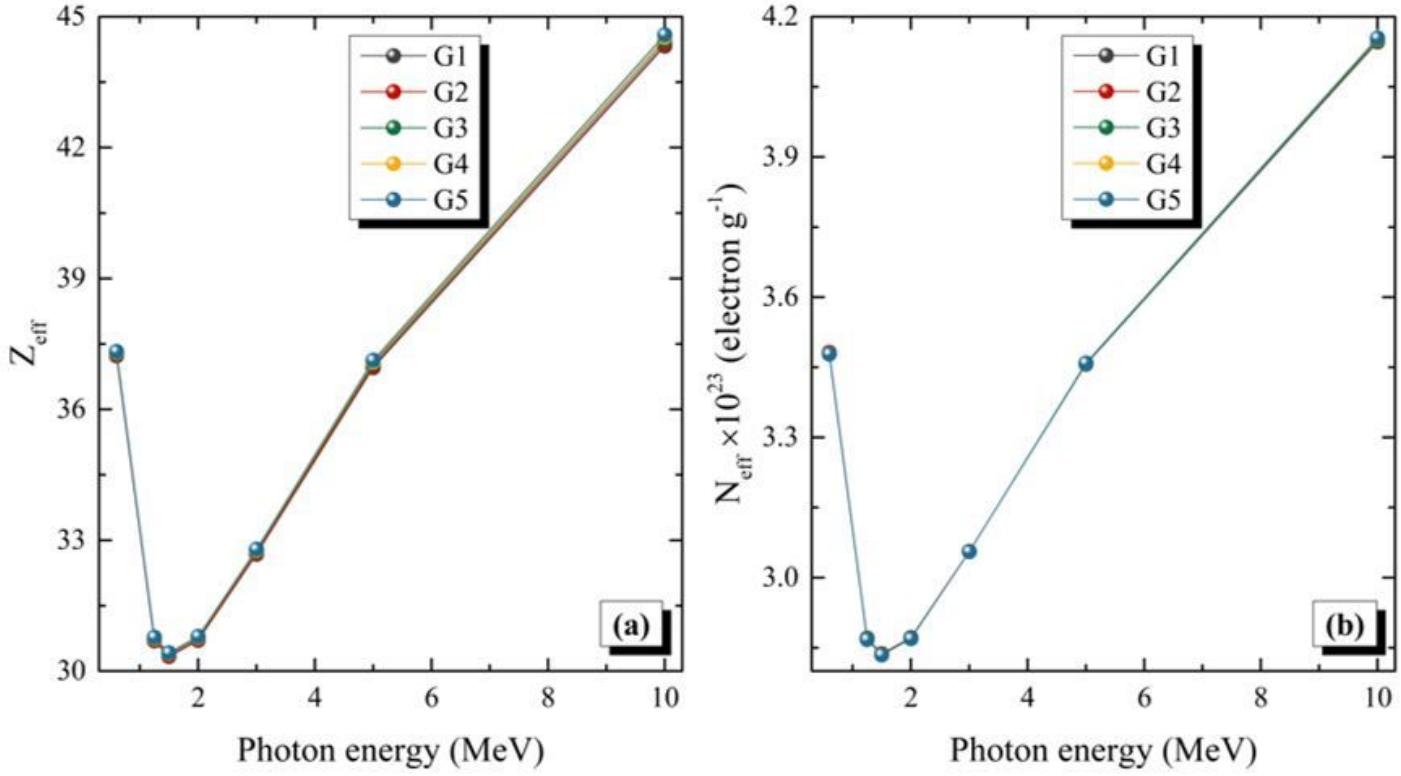

Figure 11

Photon energy dependence of the effective atomic number and effective electron density for the SiO2–Pb3O4–ZnO–WO3 glasses.

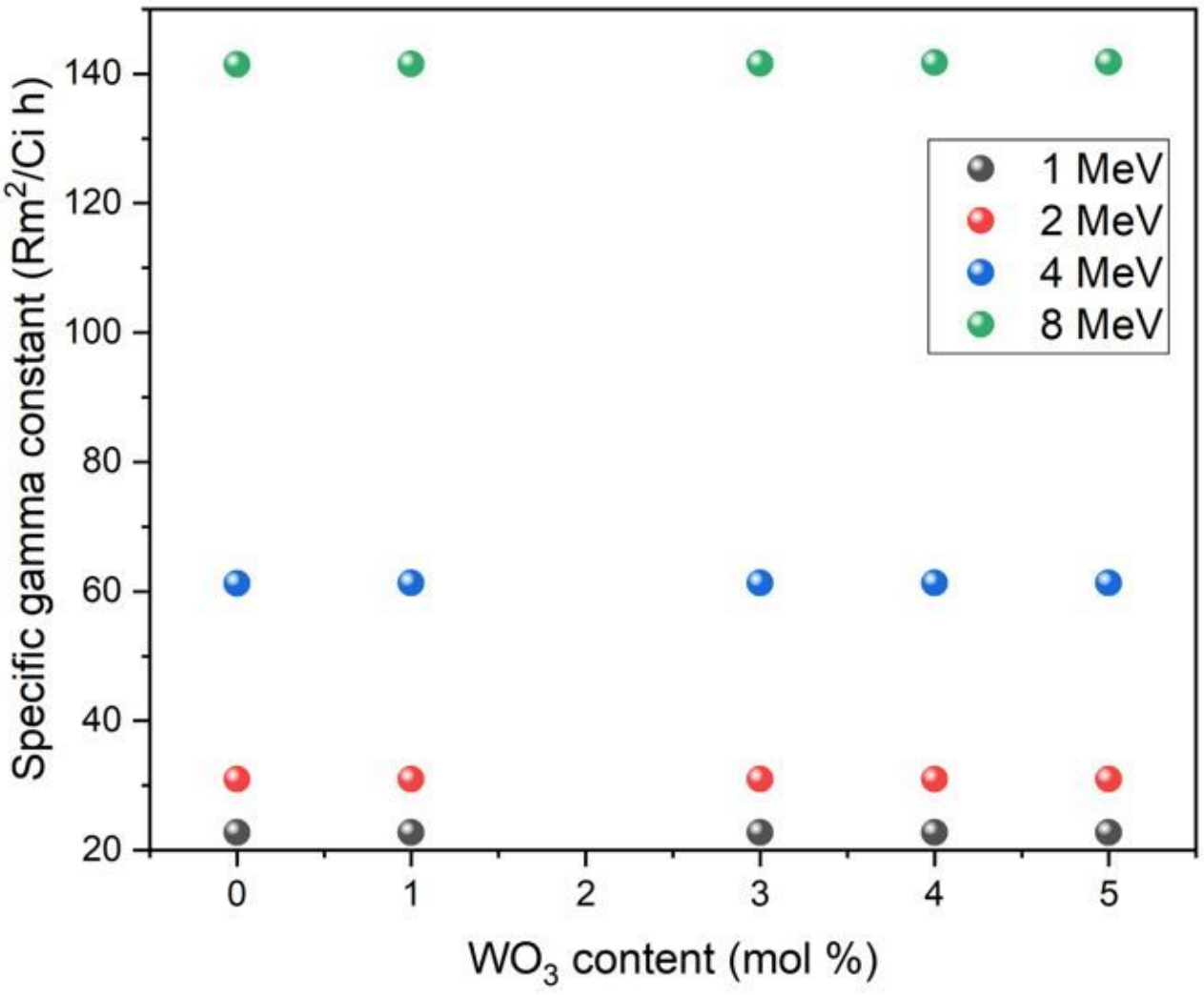

Figure 12

Specific gamma ray constant for the SiO2–Pb3O4–ZnO–WO3 glasses at different photon energies (1, 2, 4, and 8 MeV).

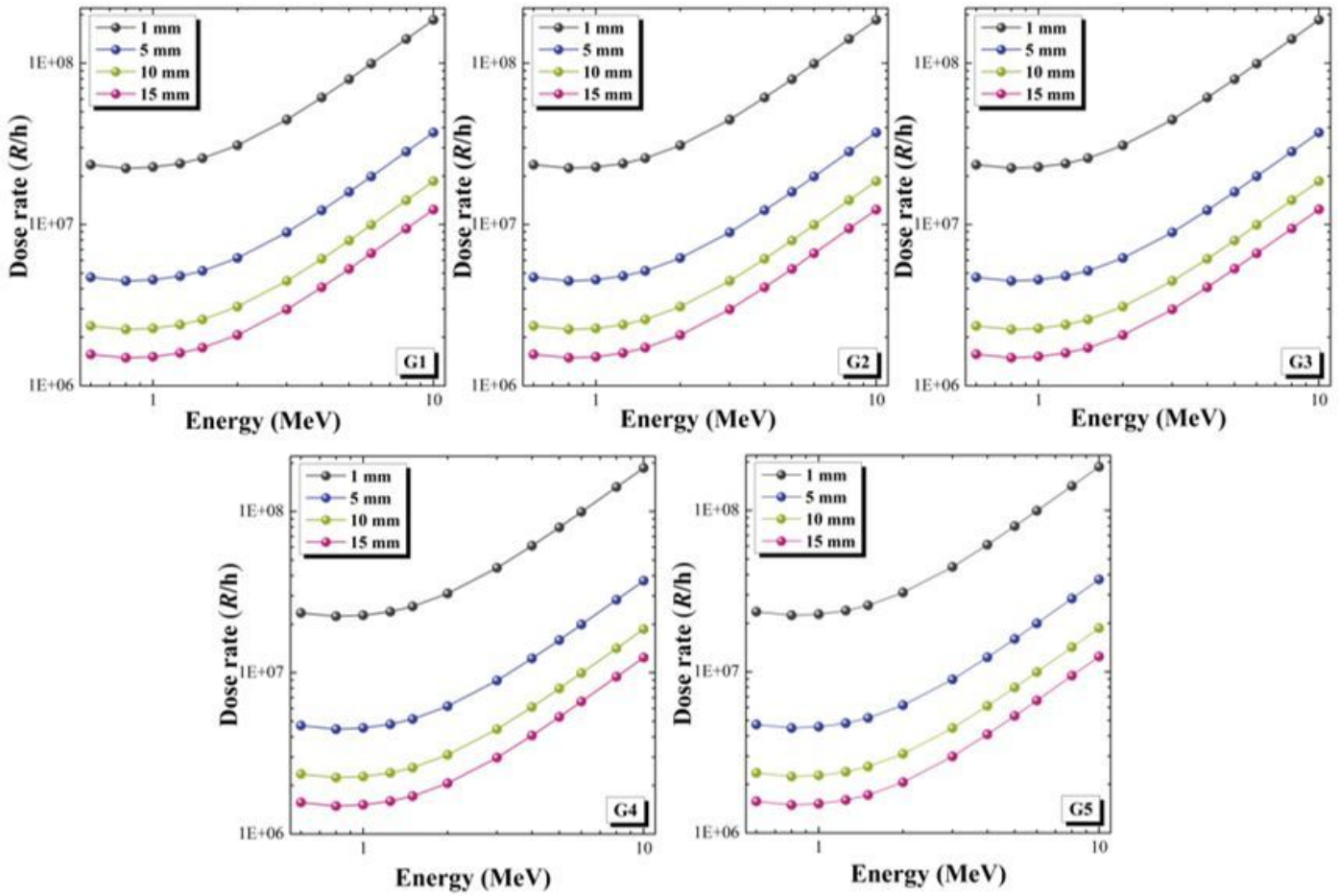

Figure 13

Variations of gamma dose rate at different energy levels for the SiO2–Pb3O4–ZnO–WO3 glasses.